Downregulation of autophagy by Met30-mediated Atg9 ubiquitination

Yuchen Feng[a,b,1], Aileen R. Ariosa[b,1], Ying Yang[a,b], Zehan Hu[c], Jörn Dengjel[c], and Daniel J. Klionsky[a,b,2]

[a]Department of Molecular, Cellular, and Developmental Biology, University of Michigan, Ann Arbor, MI 48109; [b]Life Sciences Institute, University of Michigan, Ann Arbor, MI 48109; and [c]Department of Biology, University of Fribourg, 1700 Fribourg, Switzerland

Edited by James E. Haber, Brandeis University, Waltham, MA, and approved November 21, 2020 (received for review March 24, 2020)

Macroautophagy/autophagy is a highly conserved eukaryotic molecular process that facilitates the recycling of superfluous cytoplasmic materials, damaged organelles, and invading pathogens, resulting in proper cellular homeostasis and survival during stress conditions. Autophagy is stringently regulated at multiple stages, including control at transcriptional, translational, and posttranslational levels. In this work, we identified a mechanism by which regulation of autophagy is achieved through the posttranslational modification of Atg9. Here, we show that, in order to limit autophagy to a low, basal level during normal conditions, Atg9 is ubiquitinated and subsequently targeted for degradation in a proteasome-dependent manner through the action of the E3 ligase Met30. When cells require increased autophagy flux to respond to nutrient deprivation, the proteolysis of Atg9 is significantly reduced. Overall, this work reveals an additional layer of mechanistic regulation that allows cells to further maintain appropriate levels of autophagy and to rapidly induce this process in response to stress.

autophagy | degradation | lysosome | ubiquitination | vacuole

One of the main features of autophagy is the formation of the phagophore, a dynamic and transient compartment that sequesters cytoplasmic materials destined for degradation. As the phagophore matures, it continues to expand to fully engulf its substrates, forming an enclosed double-membrane spherical structure referred to as an autophagosome (1). At present, over 40 unique autophagy-related (*ATG*) genes have been identified in eukaryotic organisms. This includes genes encoding a subset of protein components essential to autophagosome formation, collectively referred to as the "core machinery." However, despite the key advances brought about by autophagy research in past decades, many questions still remain regarding the mechanism of autophagosome biogenesis, including the source of the membrane used for nucleation and what key elements govern the kinetics of phagophore expansion and maturation.

Among the proteins in the autophagic core machinery, Atg9 is the sole transmembrane protein (1–3). Unlike most other Atg proteins, Atg9 is found at multiple punctate structures in yeast cells in addition to the phagophore assembly site (PAS)—the site of phagophore nucleation. In contrast, other Atg proteins either exist as diffuse populations in the cytosol or localize in distinct puncta that correspond to the PAS. Furthermore, various studies have shown that Atg9 travels to and from and/or remains in close proximity to the endoplasmic reticulum, the Golgi apparatus, endosomes, and mitochondria (4–6). When autophagy is induced, the percent of the total Atg9 population that localizes to the PAS is significantly increased (7, 8). These observations suggest that, during autophagy, Atg9 is constantly cycling between the PAS and peripheral sites, presumably facilitating the delivery of membranes from donor organelles that are used in autophagosome formation (2, 3). Therefore, thorough characterization of Atg9 is crucial to a comprehensive understanding of how lipids are sourced and delivered to expanding phagophores during autophagy.

Autophagy is a highly conserved, constitutive process that is carefully regulated; disruption of balanced autophagy levels leads to various diseases that include neurodegeneration, cancer, and infection, as well as aging-related disorders (9–12). It is essential that we gain a detailed understanding of the regulatory mechanisms that control autophagy, to enable its safe modulation in therapeutics. The level of Atg9 protein is increased upon nutrient deprivation; the surge in Atg9 levels is attributed to the activation of *ATG9* transcription, which is typically repressed under nutrient-rich conditions (13). An understanding of *ATG9* gene regulation is crucial in delineating the overall architecture of how autophagy levels are modulated: The amount of Atg9 protein in the cells directly correlates with the number of autophagosomes formed (13). This observation supports the purported role of Atg9 as playing a key role in orchestrating membrane delivery required in the generation of phagophores.

In addition to transcriptional control, posttranslational modifications (PTMs), such as glycosylation, ubiquitination, phosphorylation, acetylation, and lipidation, and also proteolysis, represent a subset of regulatory mechanisms that are critical for controlling the level of autophagy activity that allows cells to adapt to various stress conditions (14–16). Ubiquitination involves the addition of the 8-kDa ubiquitin (Ub) moiety to the ε amino group of lysine residues in a targeted protein; varying Ub linkages either direct the target for degradation to the 26S proteasome or vacuole/lysosome, or act as a signaling molecule for a multitude of cellular processes. The addition of ubiquitin requires a reaction cascade involving an E1 Ub activating enzyme, an E2 Ub conjugating enzyme (E2), an E3 Ub ligase, and, in some cases, an E4 Ub chain elongation factor (17, 18). Recent studies have reported a role for the CUL3–KLHL20 complex, a ubiquitin ligase in mammalian cells, in autophagy: The activity of this enzyme leads to the degradation of the PIK3C3/VPS34 and

Significance

Macroautophagy/autophagy removes surplus and/or dysfunctional cellular components for recycling in the lysosome/vacuole. During times of stress, autophagy is upregulated to ensure survival. A set of autophagy-related (Atg) proteins act in concert in a highly regulated manner to ensure proper levels of autophagy; aberrant induction of this process is correlated with numerous diseases. In this work, we show a nuanced mechanism by which autophagy is kept at a basal level via the ubiquitin–proteasome system-dependent reduction of Atg9, a transmembrane protein essential to autophagy.

Author contributions: Y.F., A.R.A., Y.Y., Z.H., J.D., and D.J.K. designed research; Y.F., A.R.A., Y.Y., and Z.H. performed research; Y.F., A.R.A., Y.Y., Z.H., J.D., and D.J.K. analyzed data; and Y.F., A.R.A., J.D., and D.J.K. wrote the paper.

The authors declare no competing interest.

This article is a PNAS Direct Submission.

[1]Y.F. and A.R.A. contributed equally to this work.

[2]To whom correspondence may be addressed. Email: klionsky@umich.edu.

This article contains supporting information online at https://www.pnas.org/lookup/suppl/doi:10.1073/pnas.2005539118/-/DCSupplemental.

Published December 21, 2020.

ULK1 complexes, and the subsequent down-regulation of autophagy (19). Lys63-linked ubiquitination of BECN1 by TRAF6 regulates its binding to BCL2 and the activity of the phosphatidylinositol 3-kinase complex. TRAF6-mediated ubiquitination of BECN1 also amplifies lipopolysaccharide-, IFNG/IFNγ- and amino acid starvation-induced autophagy in mouse macrophages (20). Similarly, CUL4-dependent ubiquitination of AMBRA1 acts to limit autophagy, whereas AMBRA1 binding to CUL5 causes stabilization of the MTOR inhibitor DEPTOR (21). In addition, deubiquitinating enzymes such as USP10 and USP13 are involved in regulating BECN1 ubiquitination in human and mouse cells, promoting autophagy activity (22). In our study, we show that Atg9 protein turnover is mediated by the ubiquitin–proteasome system (UPS). This molecular event plays a direct role in limiting the amount of autophagy in basal conditions, and termination of ubiquitination allows cells to adapt to environmental stresses by rapidly triggering an appropriate autophagic response facilitated by a sharp and swift increase in Atg9 protein levels.

Results

Atg9 Is Ubiquitinated in Nutrient-Rich Conditions. In a study by Radivojac et al. (23), the authors performed a large-scale analysis of the entire yeast proteome to analyze and predict possible ubiquitination sites in proteins. Their results indicated that yeast Atg9 is potentially ubiquitinated and is relatively short lived. Their proposed sites for ubiquitination, Lys113 and Lys138, are both localized at the intrinsically disordered N terminus of Atg9 and predicted to face the cytosol (Fig. 1*A*) (23, 24). Indeed, in a recently published paper, Atg9 protein level was shown to be regulated in a proteasome-dependent manner (25).

To further verify that Atg9 ubiquitination occurs at an endogenous level, we used tandem ubiquitin binding entities (TUBEs) agarose beads to isolate and detect polyubiquitinated Atg9 (26). Due to the low abundance of Atg9 molecules in the cell, we included an extra step of Atg9-MYC affinity isolation using anti-MYC magnetic beads to enrich Atg9 from the cell extract, and used the resulting isolate as input for the subsequent TUBEs precipitation. We refer to this procedure as a two-step affinity isolation of polyubiquitinated Atg9. Ubc6, a known proteasome substrate, was also included as a positive control (27). Similar to Ubc6, Atg9-MYC was detected after TUBEs affinity isolation, suggesting that Atg9 is indeed ubiquitinated (Fig. 1*B*, step 2, immunoprecipitation [IP]). We repeated the affinity isolation using a gradient of TUBEs agarose beads to determine the point of saturation and found that the amount of Atg9 that was affinity isolated increased, suggesting that, even at low levels of Atg9 expression, the TUBEs beads could be saturated by polyubiquitinated Atg9 (*SI Appendix*, Fig. S1*A*). When we examined the amount of ubiquitinated Atg9 in nutrient-depleted conditions, we detected a substantial decrease in the amount of affinity-isolated (ubiquitinated) protein (*SI Appendix*, Fig. S1*A*; compare lanes 5 and 8). These results suggest that Atg9 is a ubiquitinated protein, and this ubiquitination occurs primarily in nutrient-rich conditions.

To verify that Atg9 is indeed ubiquitinated, we performed mass spectrometry. The results identified multiple Atg9 lysine residues that were ubiquitinated (Fig. 1*A* and *SI Appendix*, Fig. S1*B*). Ubiquitination at K121 and K701 was dependent on nitrogen levels in the media: They were found comparatively unmodified in starvation conditions and were primarily ubiquitinated during growing conditions. K121 is located in the intrinsically disordered N terminus, and is in very close proximity to the previously predicted sites, K113 and K138 (Fig. 1*A*). Conversely, K701 is located on a loop between the fifth and sixth alpha helices of the membrane-embedded domain that was recently shown to be on the cytosolic face of Atg9 (3). Nevertheless, we focused our studies on K121, as it is in the vicinity of the two proposed

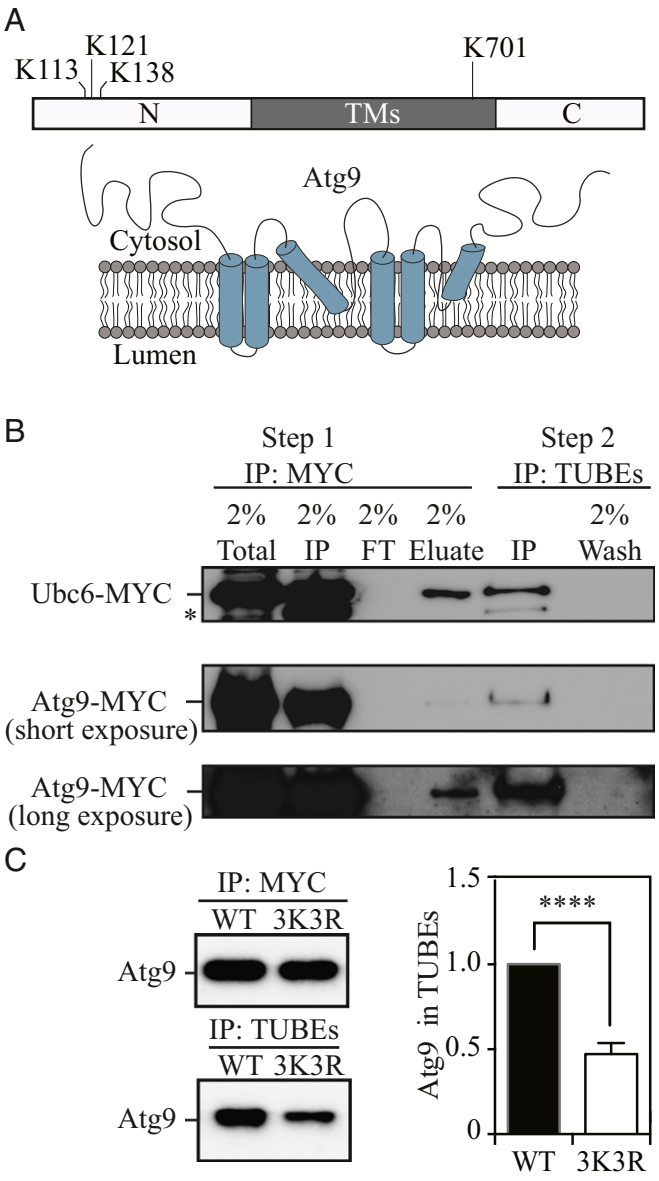

Fig. 1. Atg9 is ubiquitinated in nutrient-rich conditions. (*A*) Schematic representation of Atg9 highlighting positions of K113, K121, and K138 on the N-terminal cytosolic domain. TMs, transmembrane segments. (*B*) Two-step MYC and TUBEs affinity isolation of ubiquitinated Ubc6 and Atg9 in growing conditions. (*C*) TUBEs affinity isolation of WT Atg9-MYC and Atg9 [3K3R]-MYC. The asterisk in *B* marks a non-specific band. ****$P < 0.0001$.

ubiquitination sites (Fig. 1*A*). Furthermore, all three lysine positions (K113, K121, and K138) are conserved across different yeast species (*SI Appendix*, Fig. S1*C*). To further corroborate that these residues are posttranslationally modified, we blocked their ubiquitination by mutating these three lysines into arginines (Atg9[3K3R]) and subjected them to the same two-step affinity isolation using anti-MYC magnetic beads and TUBEs agarose beads (Fig. 1*C*). Results show that, compared to wild type (WT), a definitively reduced fraction of Atg9[3K3R] was isolated by TUBEs, indicating a substantial decrease in ubiquitination levels of the mutant protein; however, the residual binding to TUBEs beads also suggests that additional ubiquitination sites may be present, such as K701.

Atg9 Is Targeted for Proteasome-Dependent Degradation. Next, we investigated whether the ubiquitination of Atg9 is a signal for

proteasomal degradation, or if it plays a role in regulating other aspects of Atg9 function including protein movement from peripheral sites to the PAS and interaction with known binding partners. To this end, we looked at the steady-state levels of the Atg9 protein in a proteasome temperature-sensitive (ts) mutant. The *PRE1* gene encodes the beta 4 subunit of the 20S proteasome, and is essential; therefore, we used a ts *pre1-1* mutant to analyze the stability of Atg9 when proteasomal activity is compromised. To visualize Atg9 protein levels, we tagged it with the protein A epitope at the C terminus (Atg9-PA). As expected, when cultured at a permissive temperature (24 °C, proteasome active), Atg9 protein levels increased in the *pre1-1* mutant after 1 h of nitrogen starvation (Fig. 2*A*; compare lanes 1 and 2). Moreover, at a nonpermissive temperature (34 °C, proteasome inactive), the Atg9 protein level in the *pre1-1* mutant was significantly higher compared to the amount at 24 °C and did not further increase after 1 h of nitrogen starvation (Fig. 2*A*; compare lanes 1 and 3, and lanes 3 and 4). Furthermore, this increase in the amount of Atg9 protein was reversed after shifting the cells back to 24 °C (Fig. 2*A*, lane 5). Finally, in the absence of nitrogen, we detected a second Atg9 band, suggesting additional PTM such as Atg1-dependent phosphorylation (28).

To extend this analysis, we also chemically inhibited proteasomal activity by treating the cells with MG132, a proteasome inhibitor, and examined its effect on Atg9 protein turnover. In these experiments, cycloheximide (CHX) was added, allowing us to monitor degradation in the absence of new protein synthesis. In growing conditions, Atg9 protein levels were decreased down to ∼50% after 1.5 h in the presence of CHX (Fig. 2*B*; dimethyl sulfoxide [DMSO]). In contrast, this degradation was largely blocked when cells were treated simultaneously with MG132. The turnover of Ubc6 was monitored as a positive control and showed a half-life of ∼1 h (*SI Appendix*, Fig. S2), in agreement with published studies (27), and with nearly complete rescue in the presence of MG132 (*SI Appendix*, Fig. S2). Based on our findings in Fig. 1, which showed that Atg9 ubiquitination decreased in nitrogen-starvation conditions (i.e., when autophagy was induced in synthetic medium containing dextrose, but lacking nitrogen [SD-N medium]), we decided to test whether this attenuation of ubiquitination also corresponded to a decrease of degradation. Thus, we carried out the same analysis to examine degradation in the presence of CHX in nitrogen-starvation conditions and found that, indeed, Atg9 degradation was essentially blocked under autophagy-inducing conditions, even without MG132 treatment (Fig. 2*C*).

To further corroborate that the ubiquitination of Atg9 is a signal for proteasome-dependent degradation, we examined how introduction of HA-tagged ubiquitin bearing the K48R mutation affects the protein levels of Atg9. Mutation of this particular lysine to an arginine renders Ub unable to form K48-linked

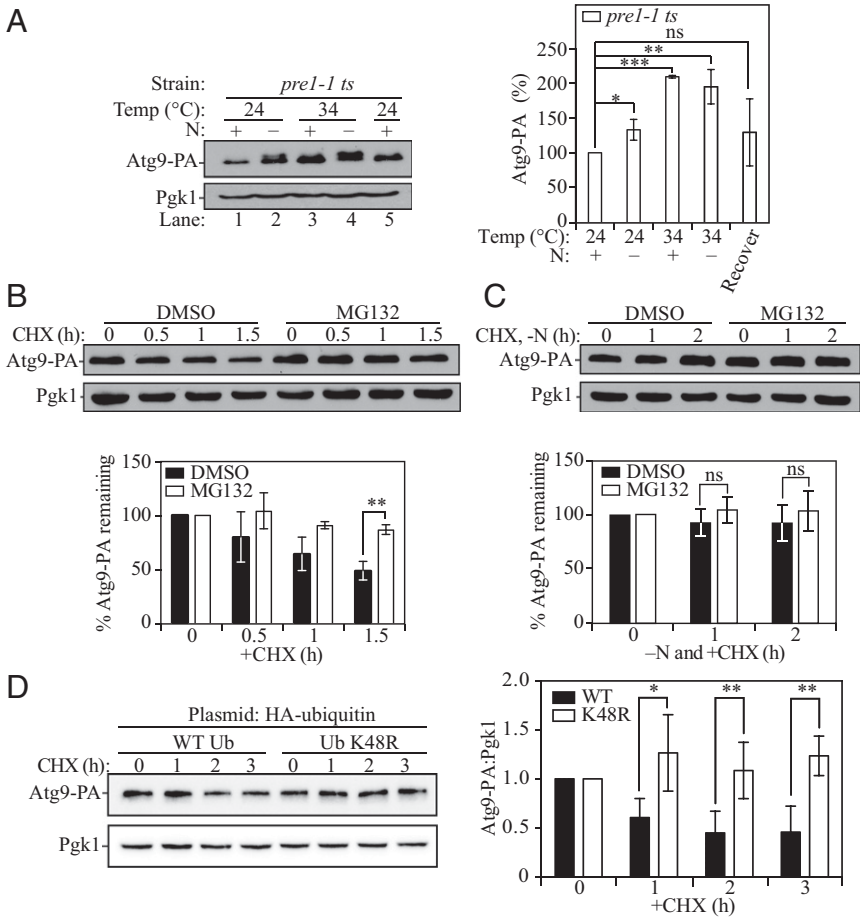

Fig. 2. Atg9 is targeted for proteasome-dependent degradation. (*A*) Atg9-PA protein levels in proteasome-mutant *pre1-1 ts* cells under permissive (24 °C) and nonpermissive (34 °C) temperatures (*Left*). Quantification of the data is shown on *Right*. (*B* and *C*) Atg9-PA protein stability after addition of CHX (100 μg/mL) in (*B*) growing or (*C*) starvation conditions in the presence of either control (DMSO) or proteasome inhibitor (MG132; 75 μM)-treated cells, which were added simultaneously. (*D*) Atg9-PA protein stability in cells expressing WT HA-ubiquitin or HA-ubiquitin K48R. Quantification of the data is shown below (*B* and *C*) or next to (*D*) each set of blots. Atg9 protein levels were normalized to endogenous Pgk1 levels. For each Atg9 variant, the amount at 0 h was defined as 100%. $*P < 0.05$, $**P < 0.01$, $***P < 0.001$.

polyubiquitin chains, which are required by the proteasome to recognize its substrates. Upon CHX treatment, levels of Atg9-PA were stabilized when a plasmid expressing HA-Ub^{K48R} was introduced into the cells (Fig. 2*D*). In contrast, in cells expressing WT HA-Ub, Atg9-PA levels were attenuated over time.

Next, we repeated the same analysis to determine whether the Atg9[3K3R] mutant, which was no longer subject to ubiquitination at these sites, remained sensitive to proteasomal degradation. In agreement with these sites serving as ubiquitination targets, the Atg9[3K3R] mutant displayed substantial stabilization of the Atg9 protein level after 3 h of CHX treatment in nutrient-rich conditions (Fig. 3*A*). We also tested how Atg9 levels were affected with single and double lysine-to-arginine mutations (*SI Appendix*, Fig. S3 *A* and *B*). Single mutations, such as K121R and K701R, did not prevent Atg9 degradation, whereas a double mutation (K113R K138R; 2K2R) resulted in protein stabilization. These results collectively suggest that Atg9 is a target of the UPS in growing conditions, when autophagy is maintained at a basal level, and that ubiquitination occurs at multiple sites on the protein.

Atg9 Is Primarily Degraded at Peripheral Sites. Atg9 undergoes dynamic cycling during autophagy, shuttling between peripheral sites and the PAS (4, 29, 30). Anterograde trafficking from peripheral sites to the PAS is dependent on various proteins, including Atg23 and Atg27 (30, 31), whereas the retrograde trafficking from the PAS to the peripheral sites depends on Atg1-Atg13 and Atg2-Atg18 (32). To understand the timing and subcellular location of Atg9 ubiquitination, we monitored the degradation of Atg9 in *atg23Δ* or *atg1Δ* cells, wherein Atg9 is either stuck in peripheral sites or at the PAS, respectively. In *atg23Δ* cells, following CHX treatment, Atg9 was substantially degraded (Fig. 3*B*). Proteolysis of Atg9 in these conditions was blocked by the addition of MG132. The extent of Atg9 degradation in *atg23Δ* cells (Fig. 3*B*) was much greater than that seen in WT cells (Fig. 2*B*); in WT cells treated with CHX, the half-life of Atg9 was ~1.5 h (Fig. 2*B*), whereas, in *atg23Δ* cells, this value was reduced to less than 1 h. A similar observation was seen in *atg27Δ* cells (*SI Appendix*, Fig. S3*C*). In contrast, in *atg1Δ* cells, Atg9 protein levels appeared to be stabilized despite the absence of MG132 following CHX treatment (Fig. 3*C*). This result was also consistent with results in *atg18Δ* cells (*SI Appendix*, Fig. S3*D*), which have a similar effect on Atg9 localization as *atg1Δ* (32). Overall, these findings suggest that Atg9 degradation is spatially controlled, and primarily takes place when Atg9 is at peripheral sites away from the PAS.

Lack of Ubiquitination Causes an Increase in Atg9 PAS Localization Affecting Autophagy Activity. Previous studies have shown that levels of Atg9 directly correlate with the frequency of autophagosome formation, and, therefore, autophagy flux (13). Our results, thus far, have shown that proteasome-dependent degradation of Atg9 occurs at peripheral sites during growing conditions. Because the Atg9[3K3R] mutant prevents degradation of Atg9 at the peripheral sites, it is plausible that this mutation causes a greater percentage of Atg9 to localize to the PAS. To follow the movement

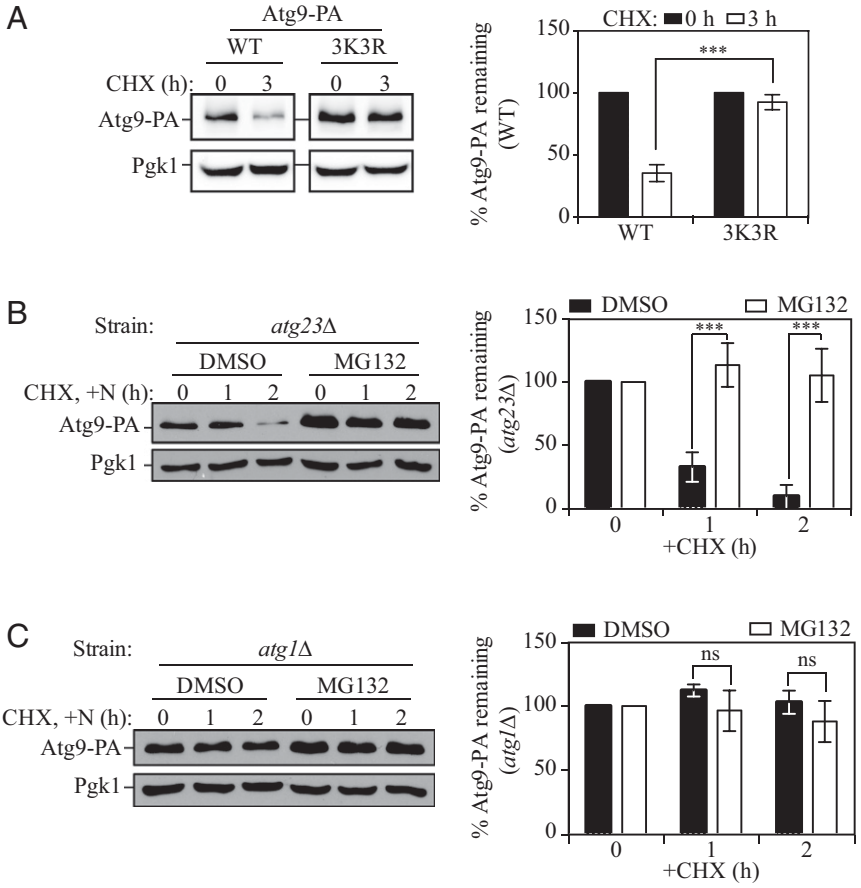

Fig. 3. Atg9 is primarily degraded at peripheral sites. (*A*) Atg9-PA protein stability in WT and 3K3R mutant cells at the indicated time points after addition of CHX. (*B* and *C*) Atg9-PA protein stability in (*B*) *atg23Δ* or (*C*) *atg1Δ* cells in control (DMSO) and proteasome inhibitor (MG132)-treatment conditions at the indicated time points after addition of CHX (*Left*). The quantification for each set of blots is shown on *Right*. Atg9 protein levels were normalized to endogenous Pgk1 levels. For each Atg9 variant, the amount at 0 h was defined as 100%. ***$P < 0.001$.

of Atg9, we monitored WT Atg9-GFP or Atg9[3K3R]-GFP localization at the PAS. Using red fluorescent protein (RFP)-tagged prApe1 (RFP-Ape1) as a marker of the PAS, we saw that, during vegetative growth, Atg9-GFP formed multiple puncta per cell, and ~25% of these puncta localized to the PAS (Fig. 4 *A* and *B*). This observed distribution pattern of Atg9 during basal autophagy agrees with our previously published data (7). The percent of GFP/RFP signal colocalization (i.e., the population of active Atg9 at the PAS) increased to ~50% after cells were shifted to starvation (–N) conditions for 30 min. In contrast, the amount of active Atg9 [3K3R]-GFP was significantly higher than WT Atg9 in growing conditions and remained at these levels after autophagy was induced (Fig. 4 *A* and *B*).

Because the Atg9[3K3R] triple mutant localized to the PAS more frequently than WT Atg9, we asked whether this mutation affected autophagy flux. To this end, we performed an assay that monitors the processing of GFP-Atg8. GFP-Atg8 is initially present on both the convex and concave surfaces of the phagophore; the GFP-Atg8 that is localized on the concave surface becomes trapped within the autophagosome, is transported into the vacuole during autophagy, and is subsequently degraded. GFP is relatively resistant to hydrolysis compared to the full-length chimera; therefore, the amount of free GFP produced reflects the level of autophagy (33). Compared to WT Atg9, the triple-mutant Atg9[3K3R] showed a statistically significant increase in autophagy-dependent GFP-Atg8 processing, particularly when looking at the 2-h nitrogen starvation (SD-N) time point (Fig. 4 *C* and *D*).

Taken together, these results suggest that limiting Atg9 degradation by blocking ubiquitination at K113, K121, and K138 leads to an increase in the population of active Atg9 that is localized to the PAS, resulting in an increase in autophagy flux after 1 h of nitrogen starvation.

Atg9 Degradation Is Mediated by Met30. The ubiquitination of Atg9 pertinent to its degradation at peripheral sites appears to be turned off during starvation. Thus, we aimed to identify the E3 ligase responsible for facilitating this PTM to understand how Atg9 levels are restrictively maintained during growing conditions. To this end, we performed a screen using yeast strains harboring knockouts or conditional mutations in the genes encoding E3 enzymes, and monitored the levels of PA-tagged Atg9 in the presence of CHX. In WT cells, after 3 h of CHX treatment, the Atg9-PA levels decreased to ~20% of that present at time 0 (Fig. 5*A*). Most of the E3 mutants that were screened, such as *yjl149wΔ* and *rad7Δ*, displayed similar Atg9 stability profiles to those seen in the WT (*SI Appendix*, Fig. S4). A few of the mutants had a partial effect on Atg9 degradation, resulting in over 50% of Atg9 being maintained at the 3-h time point. Among all of the mutants tested, the *met30-6* ts mutant displayed the most significant block; greater than 80% of Atg9 remained after 3 h in the presence of CHX (Fig. 5*A*). The *met30-9* mutant displayed a similar, although not as strong, block in degradation. This result suggests that Atg9 degradation is mediated, at least in part, by Met30.

Met30 is an F-box protein and functions as one of the substrate-recognizing components of the ubiquitin ligase complex SCF (Skp, Cullin, F-box containing) (34). The association between E3 and its potential substrates is transient due to the fact that these interactions are extremely weak. To test whether Atg9 is truly a substrate of the SCF^{Met30} ubiquitin ligase complex, we monitored their direct interaction using bimolecular

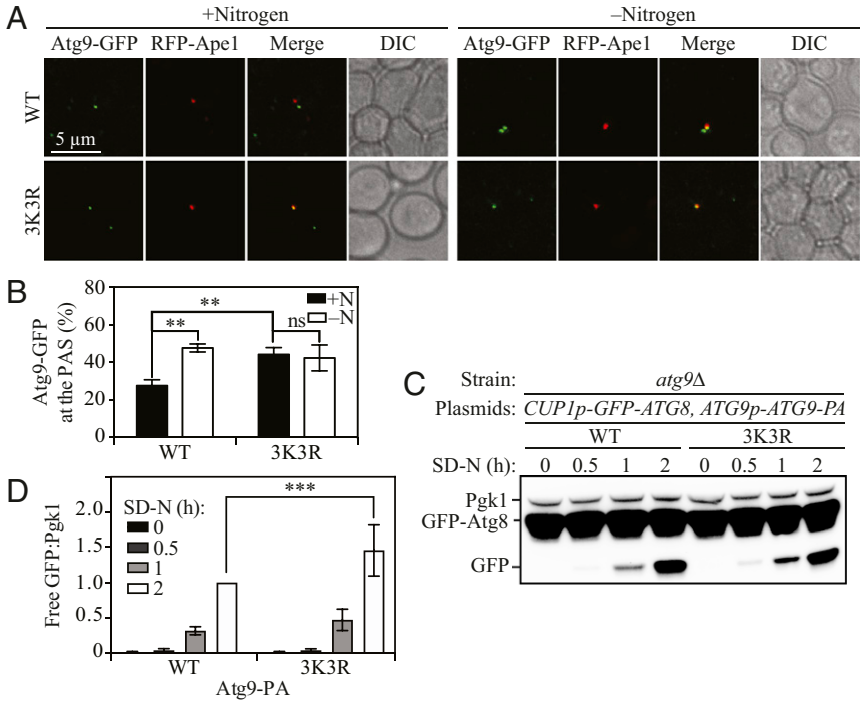

Fig. 4. Atg9 ubiquitination is important for autophagy activity. (*A*) Representative florescence microscopy images of *atg9Δ* (WT) cells transformed with a plasmid expressing WT or 3K3R mutant Atg9-GFP; the cells also contained a plasmid expressing RFP-Ape1 that serves as a PAS marker. Cells were cultured in rich medium containing yeast extract, peptone, and dextrose (YPD; 0 h) and shifted to SD-N for 30 min. The single z-stack images are displayed at equal intensity for comparison. (Scale bars: 5 μm.) (*B*) Quantification of colocalization between Atg9-GFP and RFP-Ape1 in each of the respective strains. Error bars correspond to the SD and were obtained from three independent repeats. (*C*) Western blot analysis of a GFP-Atg8 processing assay in *atg9Δ* cells transformed with a plasmid expressing WT Atg9-PA or the 3K3R mutant. These Atg9 constructs are expressed under the *ATG9* promoter. Cells were cultured in YPD, shifted to SD-N, and collected at the indicated time points of nitrogen starvation. The quantification of free GFP to Pgk1 (loading control) ratio is shown in *D*. The free GFP:Pgk1 protein ratio at the 2-h time point for WT was defined as 1. $^{**}P < 0.01$, $^{***}P < 0.001$.

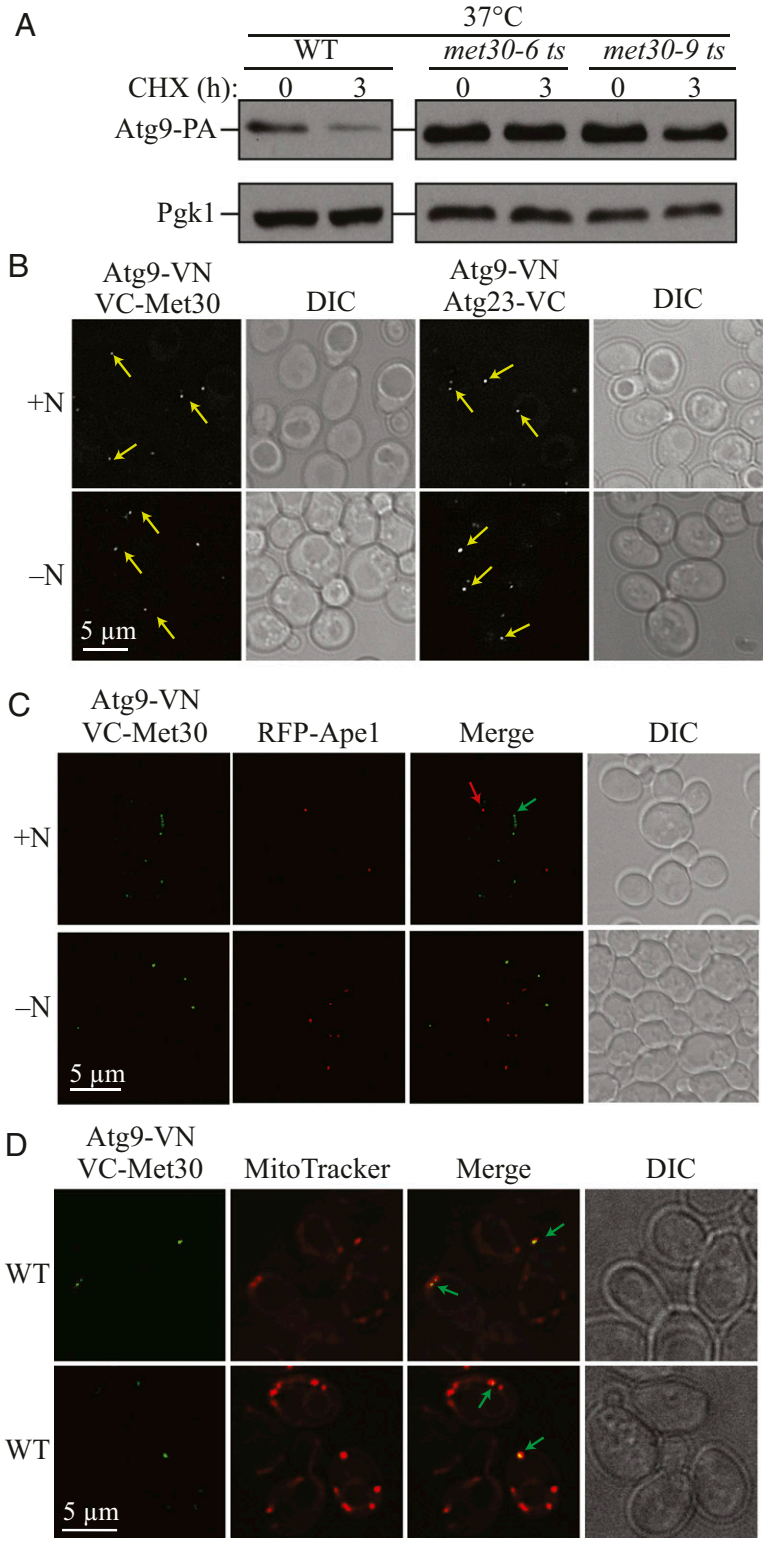

Fig. 5. Atg9 degradation is mediated by Met30. (*A*) Representative western blot images of Atg9-PA stability in two alleles of the *met30 ts* mutant. Pgk1 was used as a loading control. (*B*) Representative fluorescence microscopy images of WT cells expressing the BiFC constructs Atg9-VN and VC-Met30 cultured in YPD and shifted to SD-N for 1 h. Atg9-VN + Atg23-VC was included as a positive control. Images are from single Z sections. DIC, differential interference contrast. (Scale bar: 5 μm.) (*C*) Representative fluorescence microscopy images of WT cells expressing the BiFC constructs Atg9-VN, VC-Met30, and RFP-Ape1 cultured in YPD and shifted to SD-N for 1 h. Images are from single Z sections. (Scale bar: 5 μm.) (*D*) Representative fluorescence microscopy images of cells expressing the BiFC constructs Atg9-VN and VC-Met30 cultured in YPD and stained with MitoTracker Red CMXRos for 20 min. Images are from single Z sections. (Scale bar: 5 μm.) Yellow arrows indicate a positive BiFC signal by itself. The red arrow corresponds to the RFP-Ape1 signal (PAS marker). Green arrows show the position of a BiFC signal relative to RFP-Ape1 or MitoTracker Red.

fluorescence complementation (BiFC). Briefly, this assay involves the fusion of two halves of the Venus yellow fluorescent protein (vYFP), VN and VC, to each of the purported interacting protein partners (35). VN and VC, on their own, do not emit any fluorescence signal after excitation at 488 nm, the wavelength typically used to excite vYFP. If the two halves of vYFP are brought into close proximity due to association of the tagged target proteins, fluorescence is restored. We genomically fused VN to the C terminus of Atg9, and VC to N terminus of Met30. VC-Met30 was overexpressed using the promoter of *RPL1*. In growing conditions, a vYFP signal was observed only in cells that expressed both Atg9-VN and VC-Met30 (Fig. 5*B* and *SI Appendix*, Fig. S5*A*), suggesting that the association between Atg9 and Met30 does occur during basal autophagy conditions. The interaction of Atg9-VN and Atg23-VC was included as a positive control (Fig. 5*B*) (7). As additional negative controls, we tagged two other E3 ligases, Skp2 and Asi3, with VC at the C terminus. Unlike the result in *met30* ts strains at nonpermissive temperatures, deletion of either *SKP2* or *ASI3* did not greatly affect the Atg9-PA degradation (*SI Appendix*, Fig. S4*A*). We did not observe any vYFP signal in Atg9-VN cells that expressed either Skp2-VC or Asi3-VC (*SI Appendix*, Fig. S5*B*).

Because Atg9 traverses back and forth between the PAS and peripheral sites, we further examined where Atg9 and Met30 associate, by monitoring the location of the Atg9-vYFP-Met30 interacting signal relative to the PAS, marked by RFP-Ape1. We hypothesized that Met30 and Atg9 interact in peripheral sites because the extent of Atg9 degradation (and, presumably, its preceding ubiquitination) is greater at this locale based on the analysis of Atg9 protein levels in *atg1Δ* and *atg23Δ* cells (Fig. 3 *B* and *C*). As expected, we observed no colocalization signal between Atg9-vYFP-Met30 and RFP-Ape1 (Fig. 5*B*). To verify that Atg9 and Met30 interact prior to Atg9 trafficking to and away from the PAS, we stained yeast cells with MitoTracker Red CMXRos to visualize this specific pool of Atg9 vesicles, which localize adjacent to mitochondria (4, 36). Indeed, the Atg9-vYFP-Met30 complex colocalized with the red signal (Fig. 5*D*). This observation is consistent with our previous findings that Atg9 is primarily ubiquitinated and degraded in peripheral sites.

We previously established that, upon starvation, Atg9 ubiquitination and degradation were substantially decreased (*SI Appendix*, Figs. S1 and S2). To further understand how this is regulated, we looked at the protein levels of Met30 before and after starvation. We found that the level of Met30-PA increased after starvation (*SI Appendix*, Fig. S5*C*), which fits with the observation that most protein synthesis is stopped under these conditions, and many proteins are degraded. Thus, we conclude that Met30 activity must be regulated in a nutrient-dependent manner, such that it transduces the signal to ubiquitinate Atg9 exclusively under nutrient-rich conditions.

One of the most common means to promote or inhibit subsequent protein ubiquitination is through phosphorylation (37), and, indeed, previous studies showed that Atg9 is a phosphoprotein (7, 28). Accordingly, we examined the ubiquitination-dependent degradation of Atg9 in established phosphorylation site mutants. One potential candidate is the residue Ser122, which was previously discovered to be an Atg1-independent phosphorylation site, via mass spectrometry (7). A phosphomimetic mutant, $Atg9^{S122D}$, localizes to the PAS more frequently, and therefore has a localization phenotype somewhat like that of WT Atg9 in an *atg1Δ* strain; this distribution pattern is similar to the results we observed with Atg9[3K3R] in Fig. 4*A* (7). To test whether or not phosphorylation of Ser122 is a signal for ubiquitination, we examined how this mutation affects the stability of Atg9. The results showed that Atg9[S122A] was degraded in a similar pattern as in WT cells with 1 h or 2 h of CHX treatment, whereas Atg9[S122D] protein levels were retained similar to the protein levels in an *atg1Δ* strain (Fig. 6*A*). These results suggest that phosphorylation of S122 blocks the degradation of Atg9.

Discussion

For decades, the role of Atg9 in dictating autophagosome size, and, therefore, autophagy flux, has been attributed directly to 1) its protein expression levels and 2) its ability to dynamically cycle between purported membrane sources and the PAS. How these two factors are regulated has been a monumental focus of autophagy research in recent years. The ability to fully understand how Atg9 function (hence, autophagy itself) could be modulated is key in deducing how it can be effectively and specifically targeted for therapeutic purposes. The conclusions presented in this study add a nuanced mechanistic scheme by which autophagy is regulated in cells. Based on a large-scale analysis that predicted Atg9 to be a ubiquitinated protein with a short half-life (23), we sought to verify whether and how this protein modulation reaction indeed takes place in vivo, by using several methods. First, by employing a two-step affinity isolation assay involving TUBEs agarose beads, we showed that Atg9 is ubiquitinated, and that a higher amount of Atg9 is subject to this PTM in nutrient-rich conditions compared to starvation. Second, mass spectrometry provided empirical evidence of Atg9 ubiquitination. Third, protein stability analyses of Atg9 in cells where proteasome function was compromised, either genetically or through chemical inhibition, corroborated that this ubiquitination event is a signal that allows the proteasome to limit the active pool of Atg9 during growing conditions.

We were not able to directly show that Lys113 and Lys138 are conjugated to Ub by mass spectrometry, because the tryptic peptides containing these sites are too long to be detected. Nonetheless, our analysis tangibly identified Lys121 to be covalently modified with polyubiquitins specifically in nutrient-rich conditions. This particular lysine is in close proximity to the two aforementioned residues predicted to be ubiquitinated (23). Further analyses using TUBEs and protein stability determinations (*SI Appendix*, Fig. S3*A*) indicate that Lys113 and Lys138 are indeed ubiquitinated. A single K121R mutation was not sufficient to block the reduction in Atg9 protein levels even 3 h after inhibiting protein translation, whereas the double mutant, Atg9 [2K2R], where lysines 113 and 138 were altered into arginines, showed a comparable stabilization of protein levels as seen with Atg9[3K3R] (*SI Appendix*, Fig. S3*A*). These results are not surprising, as the UPS system is thought to use multiple signals (termed degrons) to target its substrates (38). Atg9 seemingly fits all of the categories proposed under a "tripartite model" by which protein degradation is facilitated by the UPS (38): 1) Atg9 contains a peptide motif(s) primary degron signal (as evidenced by its identification using UbPred and conservation of these residues among different species of fungi; *SI Appendix*, Fig. S2); 2) the presence of a secondary neighboring ubiquitinated site(s) (this work and UbPred); and 3) these lysines are located in an intrinsically disordered region in the N terminus of Atg9, which allows for unimpeded, effective proteasomal contact.

In general, the complexity of degrons allows for very specific regulatory control, both temporally and spatially (38, 39). This is consistent with the revelation that Atg9 is preferably degraded at peripheral sites rather than at the PAS. The association of Atg9 with Met30 was only explicitly observed for Atg9 proteins that are not at the PAS. Furthermore, degradation of Atg9 is temporally regulated because ubiquitination, and thus degradation by the proteasome, is profoundly limited during nitrogen starvation. The spatial and temporal regulation of Met30-facilitated ubiquitination of Atg9, therefore, raises a critical question: What prevents Atg9 from being accessed by SCF^{Met30} and the UPS at the PAS? What is the key signal that mediates the attenuation of this particular PTM on Atg9? The N terminus of Atg9 interacts with the Atg13 HORMA domain (2, 40, 41), and this association

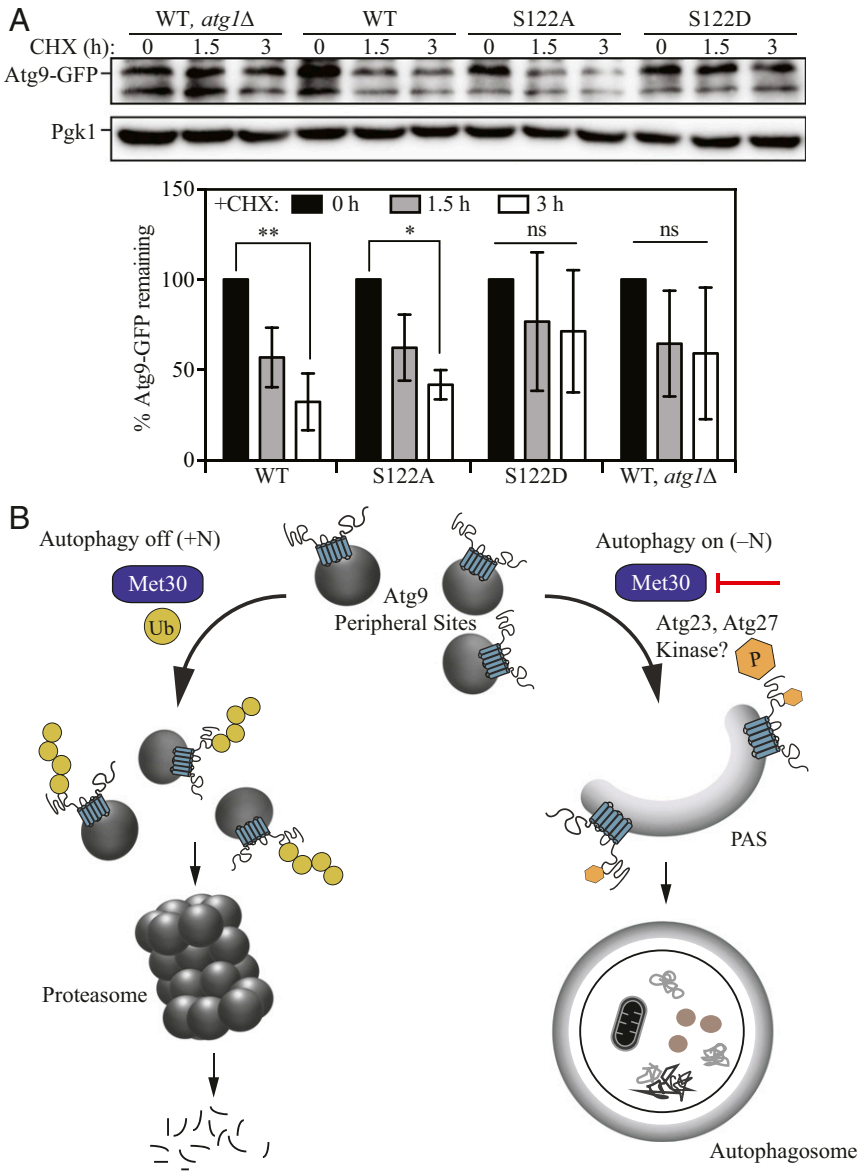

Fig. 6. Schematic model for down-regulation of autophagy through UPS-dependent degradation of Atg9. (*A*) Atg9-GFP protein stability during growing conditions for WT Atg9 ($^{+/-}$ *ATG1*), and the Atg9^{S122A} and Atg9^{S122D} mutant cells at the indicated time points after CHX addition. A quantification of the western blots is shown below the panels. Atg9 protein levels were normalized to endogenous Pgk1 levels. For each Atg9 variant, the amount at 0 h was defined as 100%. (*B*) In nutrient-rich conditions, Atg9 is synthesized, and cells are primed for autophagy. Excess Atg9 is ubiquitinated and targeted for degradation in a proteasome-dependent manner, thereby limiting autophagy to a basal level. However, when cells are nutritionally deprived, autophagy is highly induced, necessitating an increase in the amount of Atg9; the proteasome-dependent reduction of Atg9 protein levels is reduced to allow cells to induce a higher level of autophagy. $*P < 0.05$, $**P < 0.01$.

is crucial in the tethering of Atg9 vesicles by Atg13, which acts as the central hub that gathers multiple Atg proteins together to form the PAS. Perhaps the presence of Atg13 at the N terminus of Atg9 acts as a steric block that hinders its modification by SCF^{Met30}, thereby effectively mitigating Atg9 turnover. Another plausible mechanism that inhibits Atg9 ubiquitination is achieved through the phosphorylation at S122. Our results show that Atg9[S122D] is able to escape protein degradation and allows Atg9 to localize to the PAS more frequently, similar to Atg9[3K3R] (6). Intriguingly, phosphorylation at S122 occurs independently of Atg1 and is seen at a higher level during nitrogen-starvation conditions (7). The kinase responsible for this posttranslational event, and the mechanism by which phosphorylation at S122 specifically prevents ubiquitination, whether directly (i.e., by sterically blocking the action of Met30) or indirectly (i.e., due to more frequent Atg9 trafficking to the PAS), are yet to be uncovered.

In summary, we identified a mechanism by which cells regulate autophagy through ubiquitination of Atg9 (Fig. 6*B*). In growing conditions, Atg9 is synthesized in excess, presumably as a means to prime cells to carry out autophagy in a quick and efficient manner to respond to stressors. This mechanism is seen with other autophagy-related genes where certain *ATG* messenger RNAs are synthesized in excess in growing conditions, and subsequently degraded, and this degradation is blocked when cells are shifted to autophagy-inducing conditions (42). The ubiquitination of Atg9, and its subsequent turnover by the proteasome, is a simple yet very effective means of limiting autophagy to a low basal level. However, once cells are nutritionally deprived, autophagy is highly induced, necessitating an increase in the amount of Atg9. Furthermore, our

findings suggest that the "active" population of Atg9 (i.e., Atg9 that has orchestrated the delivery of membrane) at the PAS is not degraded, while that part of the Atg9 pool localized at peripheral sites is subject to degradation. Therefore, the UPS-mediated turnover of Atg9 provides cells with a nuanced layer of control that allows it to maintain appropriate levels of autophagy, while simultaneously allowing a rapid response to adapt to environmental stresses.

Materials and Methods

Strains, Media, and Growth Conditions. Yeast strains used in this paper are listed in Table 1 (7, 43, 44). Gene deletions or integrations were performed using standard methods (45, 46). Cells were cultured in rich medium (YPD; 1% [w:v] yeast extract [ForMedium, YEM04], 2% [w:v] peptone [ForMedium, PEP04], and 2% [w:v] glucose), or synthetic minimal medium (SMD; 0.67% yeast nitrogen base [ForMedium, CYN0410], 2% glucose, and auxotrophic amino acids and vitamins as needed) as indicated, referred to as nutrient-rich conditions. Autophagy was induced through nitrogen starvation by shifting cells in midlog phase from YPD (or SMD) to SD-N (0.17% yeast nitrogen base without ammonium sulfate or amino acids [ForMedium, CYN0501], and 2% [w:v] glucose) for the indicated times, referred to as starvation conditions.

Plasmids. Integrating plasmids encoding Atg9-GFP under a constitutive promoter (13) and a centromeric plasmid encoding pCu-GFP-Atg8 or RFP-Ape1 have been published previously (33). To construct the *pRS406-ATG9p-ATG9-PA* plasmid with Atg9-PA expressed under the control of the endogenous *ATG9* promoter, the GFP tag was deleted and exchanged with PA using FastCloning (47). The plasmids encoding Atg9-GFP and Atg9-PA with mutations K113R, K121R, K138R, and K701R were generated by site-directed mutagenesis and FastCloning. Mutant and WT Atg9 plasmids were linearized using StuI and integrated into the *atg9Δ* strains listed in Table 1 (47, 48).

Two-Step Affinity Isolation of Polyubiquitinated Atg9.

Step 1. Yeast cells (50 OD_{600} units; equivalent to 50 mL of cells at optical density at 600 nm [OD_{600}] = 1.0) grown in YPD were lysed using glass beads in 1.5 mL of IP buffer (phosphate-buffered saline, pH 7.4, 200 mM sorbitol, 1 mM $MgCl_2$, 0.1% Tween 20), supplemented with a mixture of protease inhibitor mixture (cOmplete™ EDTA-free, Roche; 1 tablet per 50 mL of lysis buffer) and 1 mM phenylmethylsulfonyl fluoride. After mixing by vortex for 8 min and centrifugation for 10 min at 15,000 rpm (20,879 × *g*), the resulting supernatant was removed and incubated with 100 μL of anti-MYC/c-Myc magnetic beads (Thermo Fisher Scientific) for 4 h at 4 °C. Magnetic beads were washed three times with IP buffer and collected using a magnetic stand. MYC-tagged protein was eluted using 100 μL of 0.5 mg/mL MYC/c-Myc peptide (Sigma) at 37 °C under gentle nutation. After 10 min of incubation, the eluate was collected using a magnetic stand into a fresh tube. This elution step was repeated three times, and the eluted samples were pooled together. The final eluate concentration was measured using a NanoDrop (Thermo Fisher Scientific).

Step 2. The eluate was incubated with agarose-TUBEs beads (LifeSensors) according to the manufacturer's protocol overnight at 4 °C. Beads were washed three times with IP buffer and then suspended in sodium dodecyl sulfate (SDS) polyacrylamide gel electrophoresis loading buffer (50 mM Tris-Cl, pH 6.8, 100 mM dithiothreitol, 2% SDS, 0.1% bromophenol blue, 10% glycerol) and analyzed by western blot.

Sample Preparation and Mass Spectrometry. Purified ATG9 was directly digested on beads overnight according to the filter-aided sample preparation (FASP) protocol, and the analysis was carried out essentially as described previously (49).

Additional Assays. GFP-Atg8 processing, western blot, fluorescence microscopy, and BiFC assays were performed as described previously (7, 33). All experiments other than fluorescence microscopy utilize Atg9, WT, and mutants, expressed under the endogenous *ATG9* promoter. To visualize the mitochondria, we incubated yeast cells in 0.05 μM MitoTracker Red CMXRos (Thermo Fisher Scientific) dissolved in DMSO for 20 min at 30 °C, 250 rpm, prior to taking images. [Antibodies against YFP, Atg9 and Pgk1 (a generous gift from Jeremy Thorner, University of California, Berkeley, CA) were used as described previously (29).] A commercial antibody that reacts with protein A (Jackson Immunoresearch) was used at 1:40,000 dilution, and anti-MYC/c-Myc (Invitrogen) was used at 1:5,000 dilution.

Table 1. Yeast strains used in this study

Name	Genotype	Source
ARA113	WLY176 *pdr5Δ::HIS ATG9* ^{K113R,K121R,K138R}*-MYC::TRP1*	This study
ARA114	WLY176 *atg9Δ::LEU2 ATG9*^{K113R,K121R,K138R}*-GFP::URA RFP-APE1:TRP1*	This study
ARA115	WLY176 *ASI3-VC::TRP ATG9-VN::HIS3*	This study
ARA116	WLY176 *SKP2-VC::TRP ATG9-VN::HIS3*	This study
SEY6210	MATα *leu2-3,112 ura3-52 his3-Δ200 trp1-Δ901 suc2-Δ9 lys2-801 GAL*	(43)
YKF001	WLY176 *atg9Δ::LEU2 ATG9-GFP WT::URA3*	(7)
YKF002	WLY176 *atg9Δ::LEU2 ATG9-GFP S122A::URA3*	(7)
YKF003	WLY176 *atg9Δ::LEU2 ATG9-GFP S122D::URA3*	(7)
YKF083	WLY176 *atg9Δ::LEU2 ATG9-GFP::URA RFP-APE1:TRP1*	This study
YKF496	WLY176 *atg9Δ::LEU2 ATG9-GFP::URA3 RFP-APE1::TRP1 atg1Δ::HIS3*	This study
YKF500	WLY176 *atg9Δ::LEU2 ATG9-GFP::URA3 RFP-APE1::TRP1 atg27Δ::HIS3*	This study
YKF508	WLY176 *pdr5Δ::KAN ATG9-PA::HIS3*	This study
YKF512	BY4741 *ATG9-PA:: HIS3*	This study
YKF513	BY4741 *pre1-1ts::KAN ATG9-PA::HIS3*	This study
YKF515	BY4741 *UBC6-PA::HIS3 pdr5Δ::KAN*	This study
YKF527	WLY176 *atg9Δ::LEU2*	This study
YKF528	WLY176 *pdr5Δ::KAN ATG9-PA::HIS3 atg1Δ::URA*	This study
YKF530	WLY176 *pdr5Δ::KAN ATG9-PA::HIS3 atg23Δ::URA*	This study
YKF531	WLY176 *pdr5Δ::KAN ATG9-PA::HIS3 atg27Δ::URA3*	This study
YKF535	WLY176 *pdr5Δ::KAN atg9Δ:LEU2*	This study
YKF539	WLY176 *ATG9-MYC::TRP1 doa4Δ::KAN*	This study
YKF547	WLY176 *pdr5Δ::KAN ATG9-PA::HIS3 atg18Δ::URA3*	This study
YKF548	WLY176 *pdr5Δ::KAN UBC6-13MYC::HIS3*	This study
YKF555	WLY176 *pdr5Δ::HIS ATG9-MYC::TRP1*	This study
YKF557	WLY176 *pdr5Δ::KAN UBC6-MYC::HIS3*	This study
YKF621	WLY176 *pRPL-VC-MET30::KAN*	This study
YKF631	WLY176 *ATG9-VN::HIS3*	This study
YKF640	WLY176 *pRPL-VC-MET30::KAN ATG9-VN::HIS3*	This study
WLY176	SEY6210 *pho13Δ pho8Δ60*	(44)

Statistical Analysis. Two-way ANOVA test was used to determine statistical significance.

*$P < 0.05$, **$P < 0.01$, ***$P < 0.001$, ****$P < 0.0001$, ns, not statistically significant.

Data Availability. All study data are included in the article and *SI Appendix*.

ACKNOWLEDGMENTS. We thank Dr. Mara Duncan (University of Michigan) and Dr. Taras Nazarko (Georgia State University) for helpful comments. This work was supported by NIH Grant GM131919 to D.J.K., and by the Novartis Foundation for Medical-Biological Research (Grant 16C221), the canton of Fribourg (Program Forschungspool_UniFr_2019), and the Swiss National Science Foundation (Grant 310030_184781) to J.D.

1. Y. Feng, D. He, Z. Yao, D. J. Klionsky, The machinery of macroautophagy. *Cell Res.* **24**, 24–41 (2014).
2. H. Yamamoto *et al*., Atg9 vesicles are an important membrane source during early steps of autophagosome formation. *J. Cell Biol.* **198**, 219–233 (2012).
3. C. M. Guardia *et al*., Structure of human ATG9A, the only transmembrane protein of the core autophagy machinery. *Cell Rep.* **31**, 107837 (2020).
4. F. Reggiori, T. Shintani, U. Nair, D. J. Klionsky, Atg9 cycles between mitochondria and the pre-autophagosomal structure in yeasts. *Autophagy* **1**, 101–109 (2005).
5. S. A. Tooze, T. Yoshimori, The origin of the autophagosomal membrane. *Nat. Cell Biol.* **12**, 831–835 (2010).
6. S. He *et al*., PtdIns(3)P-bound UVRAG coordinates Golgi-ER retrograde and Atg9 transport by differential interactions with the ER tether and the beclin 1 complex. *Nat. Cell Biol.* **15**, 1206–1219 (2013).
7. Y. Feng *et al*., Phosphorylation of Atg9 regulates movement to the phagophore assembly site and the rate of autophagosome formation. *Autophagy* **12**, 648–658 (2016).
8. S. K. Backues *et al*., Atg23 and Atg27 act at the early stages of Atg9 trafficking in S. cerevisiae. *Traffic* **16**, 172–190 (2015).
9. B. Levine, G. Kroemer, Biological functions of autophagy genes: A disease perspective. *Cell* **176**, 11–42 (2019).
10. A. M. Leidal, B. Levine, J. Debnath, Autophagy and the cell biology of age-related disease. *Nat. Cell Biol.* **20**, 1338–1348 (2018).
11. A. R. Ariosa, D. J. Klionsky, Autophagy core machinery: Overcoming spatial barriers in neurons. *J. Mol. Med. (Berl.)* **94**, 1217–1227 (2016).
12. Y. Yang, D. J. Klionsky, Autophagy and disease: Unanswered questions. *Cell Death Differ.* **27**, 858–871 (2020).
13. M. Jin *et al*., Transcriptional regulation by Pho23 modulates the frequency of autophagosome formation. *Curr. Biol.* **24**, 1314–1322 (2014).
14. Y. L. Deribe, T. Pawson, I. Dikic, Post-translational modifications in signal integration. *Nat. Struct. Mol. Biol.* **17**, 666–672 (2010).
15. Y. Xie, R. Kang, D. Tang, Assessment of posttranslational modifications of ATG proteins. *Methods Enzymol.* **587**, 171–188 (2017).
16. E. Kuang, J. Qi, Z. Ronai, Emerging roles of E3 ubiquitin ligases in autophagy. *Trends Biochem. Sci.* **38**, 453–460 (2013).
17. A. Varshavsky, The ubiquitin system, autophagy, and regulated protein degradation. *Annu. Rev. Biochem.* **86**, 123–128 (2017).
18. K. Wang, R. J. Deshaies, X. Liu, Assembly and regulation of CRL ubiquitin ligases. *Adv. Exp. Med. Biol.* **1217**, 33–46 (2020).
19. C.-C. Liu *et al*., Cul3-KLHL20 ubiquitin ligase governs the turnover of ULK1 and VPS34 complexes to control autophagy termination. *Mol. Cell* **61**, 84–97 (2016).
20. C.-S. Shi, J. H. Kehrl, TRAF6 and A20 regulate lysine 63-linked ubiquitination of Beclin-1 to control TLR4-induced autophagy. *Sci. Signal.* **3**, ra42 (2010).
21. M. Antonioli *et al*., AMBRA1 interplay with cullin E3 ubiquitin ligases regulates autophagy dynamics. *Dev. Cell* **31**, 734–746 (2014).
22. J. Liu *et al*., Beclin1 controls the levels of p53 by regulating the deubiquitination activity of USP10 and USP13. *Cell* **147**, 223–234 (2011).
23. P. Radivojac *et al*., Identification, analysis, and prediction of protein ubiquitination sites. *Proteins* **78**, 365–380 (2010).
24. H. Popelka, D. J. Klionsky, Post-translationally-modified structures in the autophagy machinery: An integrative perspective. *FEBS J.* **282**, 3474–3488 (2015).
25. G. Hu *et al*., Autophagy regulator Atg9 is degraded by the proteasome. *Biochem. Biophys. Res. Commun.* **522**, 254–258 (2020).
26. R. Hjerpe *et al*., Efficient protection and isolation of ubiquitylated proteins using tandem ubiquitin-binding entities. *EMBO Rep.* **10**, 1250–1258 (2009).
27. T. Ravid, S. G. Kreft, M. Hochstrasser, Membrane and soluble substrates of the Doa10 ubiquitin ligase are degraded by distinct pathways. *EMBO J.* **25**, 533–543 (2006).
28. D. Papinski *et al*., Early steps in autophagy depend on direct phosphorylation of Atg9 by the Atg1 kinase. *Mol. Cell* **53**, 471–483 (2014).
29. T. Noda *et al*., Apg9p/Cvt7p is an integral membrane protein required for transport vesicle formation in the Cvt and autophagy pathways. *J. Cell Biol.* **148**, 465–480 (2000).
30. J. E. Legakis, W.-L. Yen, D. J. Klionsky, A cycling protein complex required for selective autophagy. *Autophagy* **3**, 422–432 (2007).
31. W.-L. Yen, J. E. Legakis, U. Nair, D. J. Klionsky, Atg27 is required for autophagy-dependent cycling of Atg9. *Mol. Biol. Cell* **18**, 581–593 (2007).
32. F. Reggiori, K. A. Tucker, P. E. Stromhaug, D. J. Klionsky, The Atg1-Atg13 complex regulates Atg9 and Atg23 retrieval transport from the pre-autophagosomal structure. *Dev. Cell* **6**, 79–90 (2004).
33. T. Shintani, D. J. Klionsky, Cargo proteins facilitate the formation of transport vesicles in the cytoplasm to vacuole targeting pathway. *J. Biol. Chem.* **279**, 29889–29894 (2004).
34. D. B. Smothers, L. Kozubowski, C. Dixon, M. G. Goebl, N. Mathias, The abundance of Met30p limits SCF(Met30p) complex activity and is regulated by methionine availability. *Mol. Cell. Biol.* **20**, 7845–7852 (2000).
35. M.-K. Sung, W.-K. Huh, Bimolecular fluorescence complementation analysis system for in vivo detection of protein-protein interaction in *Saccharomyces cerevisiae*. *Yeast* **24**, 767–775 (2007).
36. M. Mari *et al*., An Atg9-containing compartment that functions in the early steps of autophagosome biogenesis. *J. Cell Biol.* **190**, 1005–1022 (2010).
37. T. Hunter, The age of crosstalk: Phosphorylation, ubiquitination, and beyond. *Mol. Cell* **28**, 730–738 (2007).
38. M. Guharoy, P. Bhowmick, M. Sallam, P. Tompa, Tripartite degrons confer diversity and specificity on regulated protein degradation in the ubiquitin-proteasome system. *Nat. Commun.* **7**, 10239 (2016).
39. C. Grabbe, K. Husnjak, I. Dikic, The spatial and temporal organization of ubiquitin networks. *Nat. Rev. Mol. Cell Biol.* **12**, 295–307 (2011).
40. Y. Rao, M. G. Perna, B. Hofmann, V. Beier, T. Wollert, The Atg1-kinase complex tethers Atg9-vesicles to initiate autophagy. *Nat. Commun.* **7**, 10338 (2016).
41. H. Popelka, D. J. Klionsky, The molecular mechanism of Atg13 function in autophagy induction: What is hidden behind the data? *Autophagy* **13**, 449–451 (2017).
42. D. Gatica *et al*., The Pat1-Lsm complex stabilizes ATG mRNA during nitrogen starvation-induced autophagy. *Mol. Cell* **73**, 314–324.e4 (2019).
43. J. S. Robinson, D. J. Klionsky, L. M. Banta, S. D. Emr, Protein sorting in *Saccharomyces cerevisiae*: Isolation of mutants defective in the delivery and processing of multiple vacuolar hydrolases. *Mol. Cell. Biol.* **8**, 4936–4948 (1988).
44. T. Kanki *et al*., A genomic screen for yeast mutants defective in selective mitochondria autophagy. *Mol. Biol. Cell* **20**, 4730–4738 (2009).
45. U. Gueldener, J. Heinisch, G. J. Koehler, D. Voss, J. H. Hegemann, A second set of loxP marker cassettes for Cre-mediated multiple gene knockouts in budding yeast. *Nucleic Acids Res.* **30**, e23 (2002).
46. M. S. Longtine *et al*., Additional modules for versatile and economical PCR-based gene deletion and modification in *Saccharomyces cerevisiae*. *Yeast* **14**, 953–961 (1998).
47. L. Zheng, U. Baumann, J.-L. Reymond, An efficient one-step site-directed and site-saturation mutagenesis protocol. *Nucleic Acids Res.* **32**, e115 (2004).
48. C. Li *et al*., FastCloning: A highly simplified, purification-free, sequence- and ligation-independent PCR cloning method. *BMC Biotechnol.* **11**, 92 (2011).
49. X. Wen *et al*., The transcription factor Spt4-Spt5 complex regulates the expression of ATG8 and ATG41. *Autophagy* **16**, 1–14 (2019).